Icarus 209 (2010) 723–737

Contents lists available at ScienceDirect

Icarus

journal homepage: www.elsevier.com/locate/icarus

Constraints on Titan's topography through fractal analysis of shorelines

Priyanka Sharma *, Shane Byrne

Lunar and Planetary Laboratory, University of Arizona, 1629 E. University Blvd, Tucson, AZ 85721, United States

ARTICLE INFO

Article history:
Received 31 July 2009
Revised 22 April 2010
Accepted 28 April 2010
Available online 6 May 2010

Keywords:
Geological processes
Radar observations
Satellites, Surfaces
Saturn, Satellites
Titan

ABSTRACT

Titan's north polar hydrocarbon lakes offer a unique opportunity to indirectly characterize the statistical properties of Titan's landscape. The complexity of a shoreline can be related to the complexity of the landscape it is embedded in through fractal theory. We mapped the shorelines of 290 of the north polar titanian lakes in the Cassini synthetic aperture radar dataset. Out of these, we used a subset of 190 lake shorelines for our analysis. The fractal dimensions of the shorelines were calculated via two methods: the divider/ruler method and the box-counting method, at length scales of (1–10) km and found to average 1.27 and 1.32, respectively. The inferred power-spectral exponent of Titan's topography (β) from theoretical and empirical relations is found to be $\leqslant 2$, which is lower than the values obtained from the global topography of the Earth or Venus. Some of the shorelines exhibit multi-fractal behavior (different fractal dimensions at different scales), which we interpret to signify a transition from one set of dominant surface processes to another. We did not observe any spatial variation in the fractal dimension with latitude; however we do report significant spatial variation of the fractal dimension with longitude. A systematic difference between the dimensions of orthogonal sections of lake shorelines is also noted, which signifies possible anisotropy in Titan's topography. The topographic information thus gleaned can be used to constrain landscape evolution modeling to infer the dominant surface processes that sculpt the landscape of Titan.

1. Introduction

The Cassini–Huygens mission has provided conclusive evidence for the modification of Titan's landscape by a variety of different surface processes including fluvial and aeolian action, tectonics, impact cratering, lacustrine processes and mantling (fallout of solid material from the atmosphere which blankets the surface). Images sent back by the Huygens probe showed long dendritic channels and rounded cobbles at the landing site, indicating fluvial activity (Soderblom et al., 2007; Tomasko et al., 2005). Subsequent images taken by the Cassini RADAR depicted the manifestation of aeolian processes at work, in the form of extensive dune fields in Titan's equatorial regions (Lorenz et al., 2006; Radebaugh et al., 2008; Elachi et al., 2006). Mountain ranges and ridges imaged by both the RADAR and the Visual and Infrared Mapping Spectrometer (VIMS) on Cassini (Brown et al., 2004) signify the presence of active tectonics on Titan (Barnes et al., 2007; Radebaugh et al., 2007). Putative cryovolcanic features point to the link between the interior and the atmosphere of Titan (Lopes et al., 2007). The signatures of the action of such a diverse set of surface processes and the scarcity of impact craters (Lorenz et al., 2007) indicate Titan to be very active geomorphologically.

RADAR images of Titan's North Pole show the landscape to be dotted with numerous small and large, radar-dark (all references to dark and bright lakes here relate to radar-dark and radar-bright) features (Stofan et al., 2007). A number of lines of evidence, including the noise-floor level backscatter inside the features, the higher brightness temperatures over the features compared to the surrounding region and the presence of channels going in and coming out of these features; all point to them being liquid filled. Conclusive evidence for the presence of liquid in these features was provided recently in the form of ethane detection by the VIMS instrument onboard Cassini (Brown et al., 2008). More recently, transient dark features that appear in the Imaging and Science Subsystem (ISS) observations of the South Pole have been interpreted as potential lakes (Turtle et al., 2009).

On Titan, as on Earth, different surface processes can compete to influence the overall topographic properties of the landscape. Precipitation events may reduce surface roughness by triggering processes such as slumping, soil creep and the washing of debris into channels, whereas channel incision will roughen the landscape. Modeling of terrestrial fluvial processes by Chase (1992) shows that landscapes may vary in roughness as a function of scale as a result of these different processes having different efficiencies over different length scales. Although the geomorphic features on Earth and Titan are very similar, the surface materials are very different, with the bedrock being made of water ice on Titan compared to silicates on Earth, and liquid methane–ethane

* Corresponding author.
E-mail addresses: psharma@lpl.arizona.edu (P. Sharma), shane@lpl.arizona.edu (S. Byrne).

0019-1035/$ - see front matter © 2010 Elsevier Inc. All rights reserved.
doi:10.1016/j.icarus.2010.04.023

playing the role of surface fluids, in contrast to liquid water on Earth (Collins, 2005; Lunine and Atreya, 2008). Although 'bedrock' erosion can produce loose surficial debris on both bodies, Titan has an additional source of such material. Photochemical reactions beginning with the destruction of methane in the atmosphere produce ethane as the primary product as well as aerosols which settle out of the atmosphere and blanket the surface (Khare et al., 1984).

Despite the gross similarity of dominant surface processes on Earth and Titan, it is difficult to constrain terrestrial landscape evolution models on Titan without topographic data. As a result, the dominance of some processes over others over different length scales on Titan, and the way the titanian landscape might have evolved over time, as a response to these processes is not very well understood.

This paper implements a novel technique to deduce surface roughness on Titan. We take advantage of the fact that Titan has standing bodies of liquid on its surface, the shorelines of which represent topographic contour lines. Fractal theory allows one to characterize the complexity of these shorelines and relate it to the roughness of the landscape in which they are embedded. Fractal analysis alone, as is being reported in this paper, can only be used to provide a measure of relative relief, i.e., topography at shorter wavelengths (smaller spatial scales) versus that over longer wavelengths (larger spatial scales). Methods which can be used to extract a measure of absolute relief at any given length scale will be the subject of future work.

2. Statistical landscape characterization

In this section we will describe how shoreline complexity may be quantified through fractal descriptors and the assumptions inherent in this comparison. We will show how statistical descriptions of the complexity of the shoreline can be related to parameters which describe the ruggedness of the landscape.

Fractals (a term coined in the 1970s, Mandelbrot, 1982) are geometric constructs which appear invariant under magnification, a property termed self-similarity. Mathematically they are produced by recursive operators (e.g. Fig. 1) which create detail down to arbitrarily small scale. Fractal (as opposed to Euclidean) shapes have no intrinsic scale and cannot be represented analytically. Many natural shapes, including shorelines, share this property of self-similarity in a statistical sense, i.e. displaying the same level of detail at increased magnification, even while differing in exact appearance.

The complexity of a fractal shape (or natural object with self-similar properties) can be characterized by its fractal dimension. In general, a curve may be divided into N linear segments of length R or a two-dimensional surface may be divided into N squares of size R. In the simple case of a straight line, $N \alpha R^{-1}$ or for that of a flat planar area, $N \alpha R^{-2}$. In general, we can say that $N \alpha R^{-D}$. Since the perimeter (P) of such a shape will be given by $N \times R$, we can say that in the general case:

$$P \alpha R^{1-D} \tag{1}$$

where D is the fractal dimension.

For straight lines, $D = 1$. In the case of a fractal, D is not an integer, e.g. in the case of the von Koch curve shown in Fig. 1, the number of line segments increases by a factor of 4 upon each iteration whereas the length of these segments decreases by a factor of 3. Using Eq. (1) to ratio two such iterations gives:

$$D = 1 - \frac{\log\left(\frac{P_1}{P_2}\right)}{\log\left(\frac{R_1}{R_2}\right)} \tag{2}$$

So, for the von Koch fractal, $D = 1.26$, i.e. it lies part-way between a straight line and a planar object. One may consider this to reflect the fact that this complex curve fills some portion of two-dimensional space. For flat planes, $D = 2$ and Area αR^{2-D} (Voss, 1988). In an analogous way to the von Koch curve discussed above, an irregular topographic surface can be thought of filling some portion of three dimensional space (although it remains a surface) and so has a fractal dimension between 2 and 3. The fractal dimension is therefore a way to quantify the amount of detail in a curve or surface. A higher value of D represents a more complex shape, however, this does not change the topological dimension (E) of these features. In the example of the von Koch curve above, this shape (for all its complexity) remains a curve with $E = 1$.

Past studies (Richardson, 1961; Mandelbrot, 1967) have found that terrestrial coastlines can be approximated by fractal shapes. The standard approach to measuring lengths of curves like shorelines is to approximate the curve by straight line segments and add up the lengths of the segments. Smaller measuring scales are sensitive to smaller features of the shoreline, and thus yield higher values for the overall lengths. Thus, the measured length of the shorelines increases, as the measuring scale decreases. The measured perimeter (P) can be related to the measuring scale (R) by the fractal dimension (D), which varies from one shoreline to another (Eq. (1)).

In contrast to shorelines, topography is not self-similar. If one were to magnify a portion of a topographic profile, it would not appear to have similar properties to the original view. Instead, topography approximates a behavior known as self-affinity whereby the variation in elevation (ΔZ) is related to the along-profile separation (ΔX) as $\Delta Z \alpha (\Delta X)^H$, where H is the Hausdorff–Besicovitch dimension (which sometimes goes by different names in different fields) and varies between 0 and 1, such behavior is also termed fractional Brownian motion. Slopes (given by $\Delta Z/\Delta X$) are therefore proportional to ΔX^{H-1} and so are higher over shorter baselines. All else being equal, low values of H correspond to lower relief at all length scales. Low values of H however correspond to rougher landscapes in that small-scale relief is larger relative to large-scale relief than a

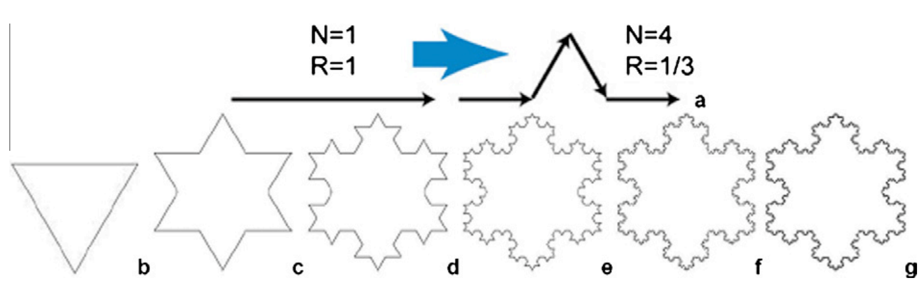

Fig. 1. Fractals are constructed with simple geometric operators, such as that shown in panel a, that rapidly produce complex shapes. In this operation, a straight line segment is replaced with 4 segments of 1/3 the original length. The results of successive iterations of this operator on an initial shape (panel b) are shown in panels c–g. This example is known as the von Koch snowflake and has a fractal dimension of log(4)/log(3) ~ 1.26 (see text for explanation).

landscape in which H is higher. It can be shown that the fractal dimension of a profile (D_1) can be related to the Hausdorff–Besicovitch dimension as $D_1 = 2 - H$ (Voss, 1988; Turcotte, 1997).

To relate the fractal dimension of the self-similar shoreline and that of the self-affine topography in which the shoreline is embedded, we make use of the concept of a zeroset (Voss, 1988; Turcotte, 1997). Like Euclidean shapes, fractals are reduced in their dimensionality by one when intersected by a plane. A zeroset is produced when you intersect an object with a plane and it has a dimensionality of one less than the original object (see Fig. 2). For example, a three-dimensional sphere intersected by a plane produces a two-dimensional circle, a two-dimensional circle intersected by a plane produces a one-dimensional line segment and a one-dimensional line segment intersected by a plane produces a zero-dimensional point. Similarly, a self-affine topographic surface $Z(x, y)$, with a fractal dimension of D_2, intersected by a horizontal plane produces a set of disconnected contour lines (Fig. 2), with a fractal dimension of D_1 equal to $(D_2 - 1)$. As the x and y coordinates of these curves are equivalent these contours are self-similar. In contrast, the intersection of this landscape with a vertical plane, producing a topographic profile, has elevation versus distance (which scale differently) and is therefore self-affine.

As the surfaces of Titan's lakes are flat, their shorelines correspond to topographic contour lines and so these curves represent a zeroset of Titan's topography. In an analogous way to the Euclidean zeroset situation above, the fractal dimension of the original landscape is given by $D_1 + 1$, where D_1 is the fractal dimension of the set of contour lines.

Another method of characterizing the roughness of topographic profiles is that of the Fourier power spectrum. Self-affine data (such as topographic profiles) have linear power spectra (in log–log space) with slopes $-\beta$ (or $-(\beta + 1)$ for the two-dimensional power spectrum). The relation between β and H (see Malamud and Turcotte (1999) for details) is given by:

$$\beta = 2H + 1 \tag{3}$$

Combining Eqs. (3) and (4) gives:

$$\beta = 5 - 2D_1 \tag{4}$$

An important distinction arises in the case of Titan where individual contour lines (lake shorelines) are available, but the full contour set is not (i.e. every depression may not be flooded with liquid). When a single contour line is available its fractal dimension is not D_1 (as a single contour is not a full zeroset), but rather $D_2/2$ (Kondev and Henley, 1995; Kondev et al., 2000; Turcotte, 1997). Thus the expected relationship is now:

$$\beta = 7 - 4\,(D_{\text{single-contour}}) \tag{5}$$

We can calculate the fractal dimension of a single shoreline using either the box-counting or ruler method (the mechanics of which are described in detail in Sections 3.3.1 and 3.3.2). These dimensions (D_B and D_R respectively) are equivalent to $D_2/2$. Thus, we can deduce the slope of the power spectrum of Titan's topography from measuring the fractal dimension of its shorelines. This allows us to quantify mathematically what is intuitive qualitatively, i.e. rugged landscapes produce complex shorelines.

In order to test these relationships we generated artificial surfaces by frequency-domain filtering of white noise. After transforming gaussian noise to the frequency domain with a fast Fourier transform (FFT) we multiplied the complex coefficients by frequency raised to the power $-(\beta + 1)/2$ before transforming them back to the spatial domain leading to a surface whose 2D power spectrum had a slope of $-(\beta + 1)$. We investigated 20 values of β between 1 and 3 and averaged the results discussed below of 50 randomly generated surfaces at each β value. We contoured these surfaces and estimated fractal dimensions from the box-counting analysis on the full contour set (D_{BS}, expected to equal D_1) and both the ruler and box-counting analysis on the longest contour (D_R and D_B, expected to equal $D_2/2$ or $(D_1 + 1)/2$).

Table 1 summarizes the various theoretical relations that we expected to hold, along with what we found empirically from this analysis. We expected that D_R should equal D_B, as these simply correspond to two independent methods of estimating the same quantity and this expectation was realized. We expected that the fractal dimension of the contour set be related to the fractal dimension of a single contour and the results in Table 1 show this to be close to correct, although the relation is not exact.

We also extracted the average slope of the power spectra from FFTs of many one-dimensional transects of these surfaces. Fig. 3 shows β derived from contour fractal dimensions versus β derived from these FFT results. When β is calculated from a full contour set, the correspondence with β derived from an FFT is close when β is less than 2.6 (i.e. this method did not work as well with the smoothest surfaces). When deriving β from a single contour the box-counting and ruler methods agree well, but not with the theoretical expectation except in the roughest cases (β close to 1). Instead, this analysis shows that β derived from contour analysis is systematically underestimated and that this underestimation grows with increasing β. In the extreme case, where β estimated from the slope of a power spectrum is 3, contour line analysis underestimates β by 10%. Fortunately, as we shall see in future sections the β values relevant to Titan are less than 2.0. Table 1 shows the best-fit linear relations between the power spectra derived βs

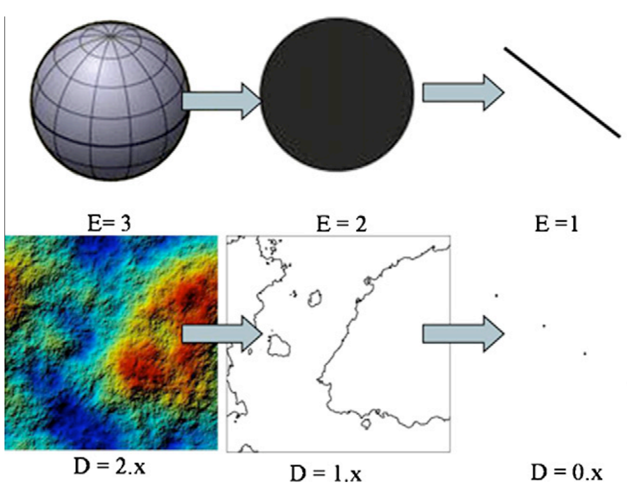

Fig. 2. Zerosets in Euclidean geometry (top row) and fractal geometry (bottom row). In both cases higher dimensional shapes are intersected by planes and their dimensionality is reduced by one. Euclidean shapes progress from a sphere to a circle to a line. Fractal shapes progress from a landscape to contour lines to a set of points (which still have fractal clustering).

Table 1
Expected and best-fit empirically derived relations between fractal dimensions of single contours D_R and D_B (for ruler and box-counting methods respectively), the fractal dimension of the contour set D_{BS} (using the box-counting method) and the FFT-derived power spectral slope of the surface β.

Relation	Theoretical	Empirical
Box versus ruler for a single contour	$D_B = 1.00D_R + 0.00$	$D_B = 0.96D_R + 0.05$
Single contour versus contour set	$D_{BS} = 2.00D_R - 1.00$	$D_{BS} = 2.15D_R - 1.25$
Beta versus contour set dimension (see Fig. 3)	$\beta = 5.00 - 2.00D_{BS}$	$\beta = 5.25 - 2.16D_{BS}$
Beta versus single contour dimension	$\beta = 7.00 - 4.00D_R$	$\beta = 7.99 - 4.69D_R$
(see Fig. 3)	$\beta = 7.00 - 4.00D_B$	$\beta = 8.21 - 4.90D_B$

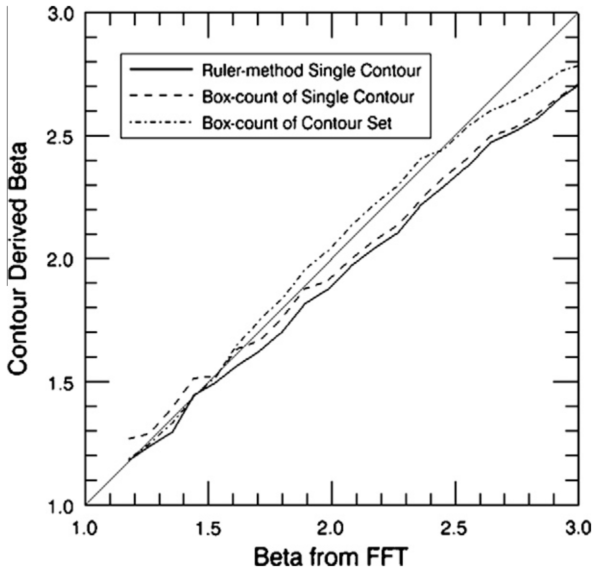

Fig. 3. Power spectral slope of artificially generated landscapes retrieved from contour analysis versus those retrieved from Fourier analysis. See Table 1 for coefficients of best-fit linear relations.

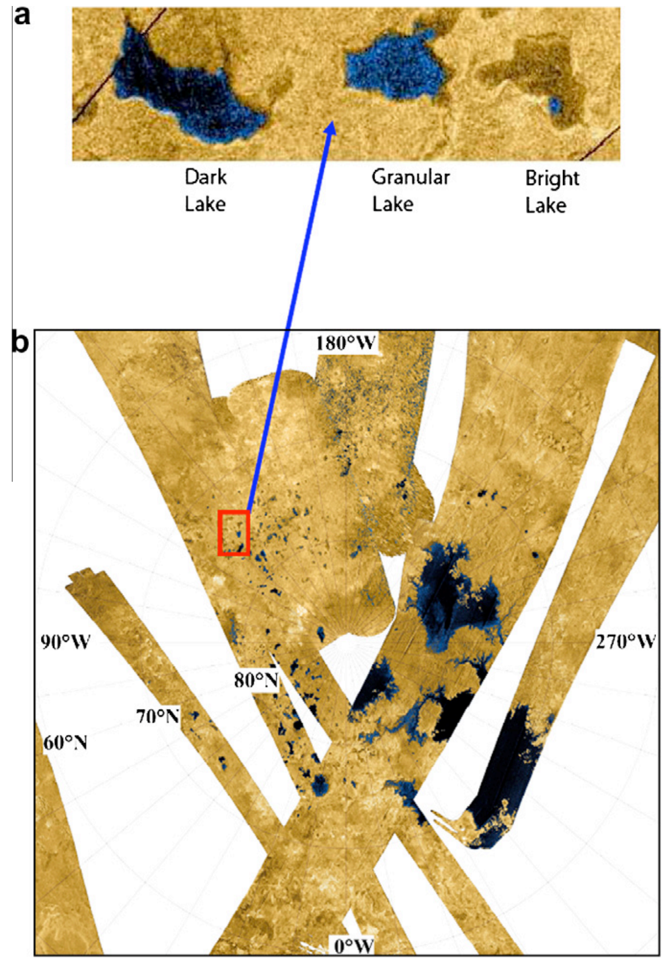

Fig. 4. (a) The basic lake-types found in Titan's north polar area. This is a false color image, created by scaling radar reflectance data. The color scale is arbitrary (not related to compositional differences), with blue corresponding to the smoothest features (with lowest radar backscatter). See description of (b) for further explanation. (b) Mosaic of north polar SAR data acquired up to May of 2007. Projection is polar stereographic with both parallels and meridians spaced every 10°. Dark blue features correspond to liquid-filled depressions. This product is 2700 km across (latitudes 60–90°N) with a resolution of 343 m/pixel (i.e. the full resolution of the constituent data is preserved). (Planetary photojournal, product ID PIA10008.). (For interpretation of the references to color in this figure legend, the reader is referred to the web version of this article.)

and contour fractal dimensions. Throughout this paper we will be analyzing single contours and in most sections we will be comparing fractal dimensions to similarly derived fractal dimensions and the departure from theory described above will not be an issue.

Fig. 3 and Table 1 show that the relationship between contour fractal dimension and β is very close to linear. Indeed, using our empirical linear relationship recovers the β of synthetic surfaces with high accuracy; however, the cause of this departure from theory is unknown at this time. This departure can also be noted in the work of other researchers e.g. Fig. 7.12 on page 156 of Turcotte (1997). They investigated the validity of Eq. (3) using one-dimensional time series. Although they describe the agreement with the theoretical relation as 'good' there is clearly a mis-match that corresponds to the one we see in Fig. 3, at high values of β and H. Later, in Section 3.3.3, we will verify the accuracy of our fractal dimension estimation codes and find both the box-counting and the ruler code to be very accurate. For now, we will use both the theoretical and our derived empirical relationship (Table 1) when converting contour fractal dimensions to power-spectral slopes later in Section 3.3.4.

An important assumption is made while characterizing topography from shoreline information. Our analysis relies on the lake edge representing a topographic contour line (i.e. being liquid filled). Titan's lakes fall into three basic types (Hayes et al., 2008), see Fig. 4a. Dark and granular lakes are interpreted to contain liquid of different depths and a smooth gradation of backscatter intensity exists between the two. Bright lakes are interpreted to be currently dry and form a distinct group when classified by backscatter intensity (Hayes et al., 2008; Pailou et al., 2008). We have avoided the bright 'lake' features many of which appear not only to be dry, but also to have the appearance of topographic sink holes (Mitchell et al., 2007) and so their boundaries may be set by mass wasting processes that have little connection with the topography of the surrounding landscape. In other words, contour lines drawn around the dark units are assumed to be typical of contour lines on the surrounding landscape, while in the case of the bright empty basins, their edges will not be representative of topographic contours on the surrounding landscape. Keeping this in mind, we mapped 290 dark liquid filled features. This sample dataset was further reduced with the size constraint described in the next two paragraphs.

An important limitation of this analysis is the limited range of spatial scales over which it can be used. The retrieved fractal dimension is only valid over a certain range of wavelengths bounded by the minimum and maximum scales we used to analyze the shorelines. The minimum scale is close to 1 km and is set by the resolution of the dataset. The smallest features that we can resolve correspond to twice the dataset resolution (Nyquist scale), i.e. 1 km, which provides the lower wavelength cutoff for our analysis. The maximum scale is set by the finite size of the lake shoreline being measured and varies from lake to lake.

For our fractal analysis to cover a useful range of spatial scales, the total perimeter of the lakes must be at least a few orders of magnitude larger than the resolution of the data, i.e., there must be many 1–10 km segments in the perimeter of a lake for our analysis to be applicable. We have therefore not considered lake features having perimeter less than 70 km, i.e. features that are less than approximately 22 km across in diameter. This further reduced our dataset of useful lake shorelines from 290 to 190. All the results presented in this paper are based on the analysis of those 190 radar-dark features, which have perimeter larger than 70 km.

3. Instrument, dataset and measurements

3.1. Cassini RADAR

The Radio Detection and Ranging Instrument (RADAR) onboard the Cassini spacecraft is a K_u-band (13.7 GHz, 2.17 cm wavelength), linearly polarized device (Elachi et al., 2004). It can function in four different operation modes: imaging (Synthetic Aperture Radar – SAR), altimetry, scatterometry and radiometry, with the first three being active modes, in which the instrument bounces pulses off Titan's surface with the aims of creating images of the surface (imaging), measuring topography (altimetry) and determining the surface properties through studying the way the surface (and sub-surface) scatters incident waves (scatterometry). The last mode, radiometry, is a passive one, in which the instrument records the energy emanating from Titan's surface.

3.2. RADAR dataset

We utilized Cassini SAR data in the form of Basic Image Data Record (BIDR) files (Stiles, 2005) as the base mapping dataset for this analysis (Fig. 4b). Cassini has had multiple Titan encounters dedicated to acquisition of SAR data and fortunately the north polar region is particularly well covered. Cassini SAR has covered 27% of the surface of Titan, during the 'prime' (nominal) mission period until June 2008 (Lorenz and Radebaugh, 2009). Almost 55% of the region above 55°N has been covered (Hayes et al., 2008). The features interpreted as lakes range in size from thousands of square kilometers to as small as 1 km^2. The resolution of the SAR swaths over these lakes ranges from $\sim$300 m at best up to 1500 m and varies mainly along the length of the images.

The first step undertaken was mapping all the north polar lakes using the GIS software, ArcMAP, from ESRI (Sharma and Byrne, 2008a,b). We attempted to develop automated methods of outlining the shorelines, including contouring of backscattered intensity, but those methods did not produce a good representation of the actual lake shorelines, prompting us to outline the lakes manually. To counter the subjectivity that the manual method might introduce in our analysis, we applied a consistent set of rules for mapping all the shorelines. Some lakes were split between different radar swaths and had straight boundaries in some sections, coinciding with the edges of the swaths (e.g. Fig. 5a). We considered such split-up lakes as two separate features with distinct shorelines and excluded the straight edges from our fractal analysis. Some lakes seemed to be filled with liquid in only one section (based on their much darker appearance in one section), whereas surrounding regions were less distinct (Fig. 5b). In such cases, we only outlined the darker liquid-filled section of the lake. Some lakes were connected by thin channels (0.5–2 km wide), in which case we considered the connected lakes as separate features, without including the connecting channel (Fig. 5c). Some lakes had complex dendritic networks surrounding them, which were included as part of the lake outlines (Fig. 5d). We manually outlined the lake shorelines at the full resolution of the dataset, a selection of which is shown in Fig. 6. To test the uncertainty introduced in the derived fractal dimension due to the subjective nature of manually outlining shoreline boundaries, we remapped a subset of the lakes in our dataset three independent times and calculated the fractal dimensions via both the ruler and the box counting techniques (described in detail in Sections 3.3.1 and 3.3.2). Table 2 shows the consistency in the derived dimensions via both the methods. The values for the ruler fractal dimensions are within ±1.5% and the box-counting dimensions are within ±1% of each

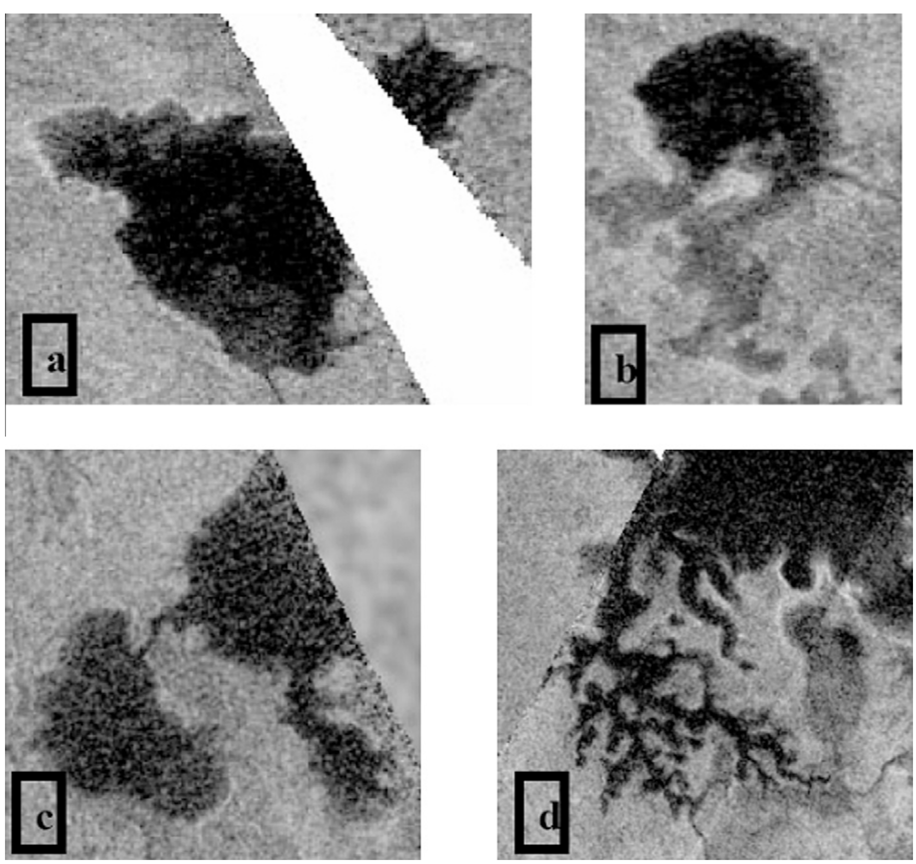

Fig. 5. Examples of cases requiring manual intervention while mapping of shorelines.

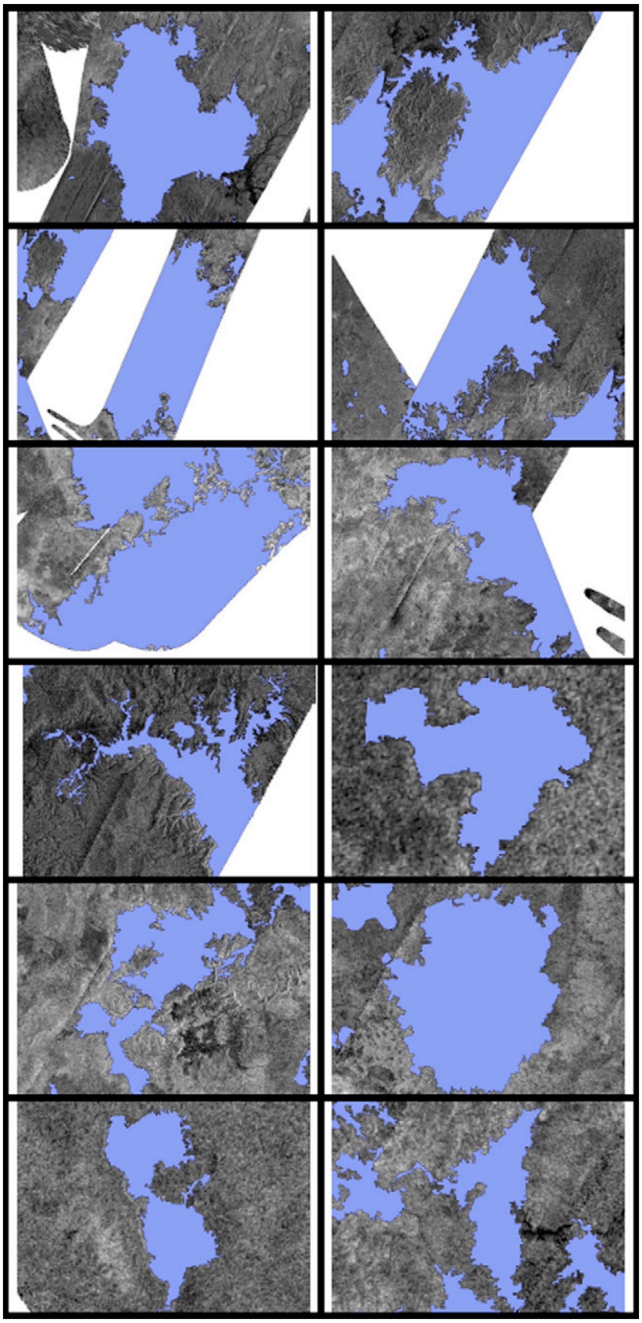

Fig. 6. Examples of some of the mapped lake features.

other for the multiple re-mappings. Thus, applying a uniform set of rules while mapping minimized the effect of subjective selection of boundaries.

Another source of discrepancy that affects mapping is systematic variations in the way different individuals would apply different sets of rules while mapping the shorelines. Since different individuals/groups working independently might subscribe to different conventions while mapping, it could lead to different results, in spite of being consistent with their own set of rules. Other groups (e.g. Hayes et al., 2008) have mapped Titan's polar lakes for their publications and there is no commonly accepted set of vectors/shapefiles for these shorelines. Currently, every group researching on Titan's polar lakes needs to map out the shorelines manually. It would thus be highly beneficial for the scientific community to agree on a common set of vectors for these surface features.

3.3. Shoreline analysis methods

There are two main methods that can be used for determining the fractal dimension of a shoreline (or shoreline segment), the divider or ruler method and the box-counting method.

3.3.1. Divider/ruler method

As described in Section 1, shorelines can be approximated as fractal shapes, with perimeter and measuring scale related by Eq. (1). Measuring the perimeter of the shoreline at many length scales (values of R) allows one to estimate D (Fig. 7a–c). A linear fit to P versus R in log–log space has a slope of $1 - D$ (Eq. (1)). In general, Titan's shorelines are well described by the power law shown in Eq. (1), and so they can be described as self-similar fractals. The data in the example, shown in Fig. 7d, show a consistent value of D over the range of spatial scales investigated (1–10 km). Such behavior was typical of the other shorelines. The range of scale lengths that we used was dependent on the size of each individual lake. We used scales as small as 2 pixels to as large as ~10% of the lake's perimeter.

An assessment of this method by Andrle (1992) shows it to be quite accurate when some common pitfalls are avoided. The common sources of error include the effect of the last partial step which invariably occurs at the end of a line being measured; the effect of varying the starting point of a divider walk on the measured perimeter; and the effect of nonlinearity in the relationship between log(perimeter) and log(measuring scale). Our code for implementing the ruler method overcomes these sources of error by (1) including the last partial step as a fractional step while calculating the perimeter, (2) calculating the perimeters with a number of different starting points and taking their average, and (3) ignoring outlier points for slope determination.

3.3.2. Box-counting method

In this method, the mapped shoreline is covered with boxes of size R. For each value of R, there is a minimum number of boxes (N) that are required to completely cover the shoreline. Our code employs an easier-to-implement version (also employed by Appleby (1996), Tatsumi et al. (1989), and Longley and Batty (1989)) of the box-counting method, in which the shoreline is covered with a grid of square boxes of size R and the number of boxes in the grid that fall on sections of the shorelines are counted (Fig. 8a–c).

For fractal shapes, there is a power-law relationship between the number of boxes required and their size. In this case, a linear fit to a plot of N versus R in log–log space has a slope of $-D$ (Turcotte, 1997), e.g. Fig. 8d. We found Titan's shorelines to exhibit this power law behavior, indicating their fractal nature.

The range of box sizes that we used was dependent on the size of each individual lake. We changed the box size as a power of two and used boxes as small as 2 pixels to as large as one-half of the lake size. We did not use the two smallest and largest box sizes for slope determination while fitting a power law to these data, following the example of Klinkenberg (1994).

We performed a simple exercise to test the sensitivity of our box-counting code to orientation of the shorelines. We rotated all the mapped shoreline shapefiles by different amounts to check if this affected the calculated fractal dimension. As can be seen from Fig. 9, rotating the lakes does not make any significant overall difference to the calculation of the fractal dimension by the box-counting code (the mean fractal dimension only varied within ±0.72% for the different rotations), which is thus inferred to be robust.

3.3.3. Generation of synthetic fractals

In order to test the accuracy of the ruler and box-counting methods against a known standard, we generated synthetic fractals

Table 2
Ruler and box-counting fractal dimensions of 15 of Titan's lake shorelines on multiple re-mappings.

Titan lake	Center latitude (°N)	Center longitude (°W)	Ruler *D*			Box counting *D*		
			1st mapping	2nd mapping	3rd mapping	1st mapping	2nd mapping	3rd mapping
1	83.54	49.80	1.24	1.23	1.24	1.18	1.18	1.19
2	84.58	31.08	1.24	1.23	1.27	1.14	1.11	1.11
3	82.10	48.64	1.25	1.24	1.25	1.18	1.16	1.16
4	84.93	−104.74	1.24	1.29	1.27	1.13	1.12	1.12
5	69.73	−114.78	1.25	1.31	1.29	1.15	1.16	1.16
6	78.22	20.66	1.25	1.25	1.25	1.14	1.14	1.13
7	78.92	122.60	1.24	1.26	1.25	1.11	1.11	1.11
8	80.35	130.48	1.24	1.23	1.22	1.11	1.11	1.11
9	77.02	129.62	1.25	1.22	1.23	1.11	1.17	1.15
10	74.17	126.04	1.26	1.27	1.26	1.10	1.10	1.10
11	80.49	120.75	1.13	1.12	1.12	1.07	1.08	1.08
12	79.61	26.10	1.21	1.22	1.21	1.10	1.09	1.10
13	70.80	−134.67	1.30	1.32	1.31	1.16	1.15	1.16
14	77.25	28.77	1.40	1.40	1.42	1.13	1.13	1.13
15	69.49	178.25	1.35	1.33	1.35	1.13	1.14	1.13

with known fractal dimensions and compared their actual dimensions with dimensions calculated via the two methods. A total of five such fractals, as shown in Fig. 10, were generated. The initiator in each case was a pentagon, each straight edge of which was replaced with the generator shape shown in the lower right inset of each fractal in Fig. 10. This replacement was repeated a number of times to obtain the resultant synthetic fractals. Fractal dimensions can be exactly calculated for these shapes using Eq. (2). The scatter plot in Fig. 10 compares the accuracy of the ruler and box-counting methods. The dimensions calculated via the ruler and the box-counting methods are in very good agreement with the theoretical dimensions, for fractals with dimensions in the range of 1.0–1.5. In the scatter plot in Fig. 10, the dotted gray line indicates 1σ range of dimensions for Titan's shorelines (1.17–1.42), the dashed gray line indicates the 2σ range (1.07–1.52) and the solid gray line indicates the 1.645σ range (1.1055–1.485), which contains 90% of the data for Titan's shorelines. As is evident from the scatter plot, the ruler method is more accurate than the box-counting method over the range of fractal dimensions within the 1.645σ box. Although 10% of the lakes fall outside this 1.645σ range, only 5% fall outside the range on the higher dimension side. Thus, we can infer from Fig. 10 that the ruler method is more reliable than the box-counting method over the range of fractal dimensions relevant to Titan (1.1055–1.485).

3.3.4. Discussion of results for Titan's shorelines

The calculated values of the mean fractal dimensions of Titan's shorelines via the box-counting (1.32 ± 0.1) and the ruler method (1.27 ± 0.1) are comparable to the previously published estimates of dimensions of terrestrial coastlines like the western coastline of Britain (1.25) (Mandelbrot, 1967). The histograms in Fig. 11 compare the results of the ruler and the box-counting method. A high value of the fractal dimension suggests the shoreline to be intricate, which implies a rugged surrounding landscape; while a low value suggests a simple shoreline, which implies a smooth surrounding landscape (see Supplementary online material, Table S1, for a list of mapped lakes, their locations and individual ruler and box-counting fractal dimensions).

Using the mean of the ruler and box-counting dimensions (1.295), we obtain a value for theoretical β as 1.82 while the average empirical relation for a single contour gives a β value of 1.89. Using the more reliable of the two dimensions: the ruler dimension of 1.27, we get the theoretical/empirical value of β as 1.92/2.03. Comparing the β value for Titan to the average β value of 2.0 determined for Earth (Rapp, 1989) and Venus (Kucinskas and Turcotte, 1994), we find Titan's landscape to be rougher at shorter wavelengths relative to longer wavelengths. There could be a number of factors responsible for this, including the lower gravity on Titan as compared to Earth and Venus, which could be responsible for lesser efficiency of diffusive (i.e. smoothing) processes like mass wasting on Titan.

4. Additional investigations

In addition to deriving the fractal dimension of the mapped lake shorelines, we undertook three other related investigations: (1) searching for multi-fractal behavior, (2) checking for spatial variation of fractal dimension and (3) examining evidence for a signature of anisotropic topography. Sections 4.1–4.3 describe each of these investigations in detail.

4.1. Multi-fractal analysis

Multi-fractal behavior implies change in the landscape from one fractal dimension to another at a certain wavelength. Such changes in topographic statistics between large and small scales signal that different sets of processes are shaping the landscape at different spatial scales (Mark and Aronson, 1984; Chase, 1992). Both the box-counting and ruler methods characterize the shoreline over a range of spatial scales. How this characterization changes with spatial scale determines the fractal dimension so it is possible to have different fractal dimensions appropriate for different sections of the total range of spatial scales investigated.

Twenty-one lakes were found to exhibit multi-fractal behavior, indicated by a change in slope of the log(perimeter) versus log(baseline) plots obtained by applying the ruler method on the shorelines (We found no change in the slope of the log(number of boxes) versus log(box size) plots obtained with the box-counting method). Fig. 12a–c shows three of these multi-fractal lakes. Fig. 12a shows an example of a multifractal shoreline with increasing slope from smaller to larger wavelengths (and thus decreasing fractal dimension, since D = 1-slope). In contrast, Fig. 12b shows an example of a multifractal shoreline with decreasing slope from smaller to larger wavelengths (and thus increasing fractal dimension). Eight of the multi-fractal lake shorelines (e.g. Fig. 12c) also exhibit multiple breaks in slope. The cross-over point from one fractal dimension to another lies over a small range of (2–3.5) km for the larger multi-fractal lakes (area >250 km^2) and varies over a much wider range (2.2–7 km) for the smaller multi-fractal lakes (area <250 km^2).

Interpreting these breaks in slopes requires an understanding of the effect of various surface processes on the roughness and

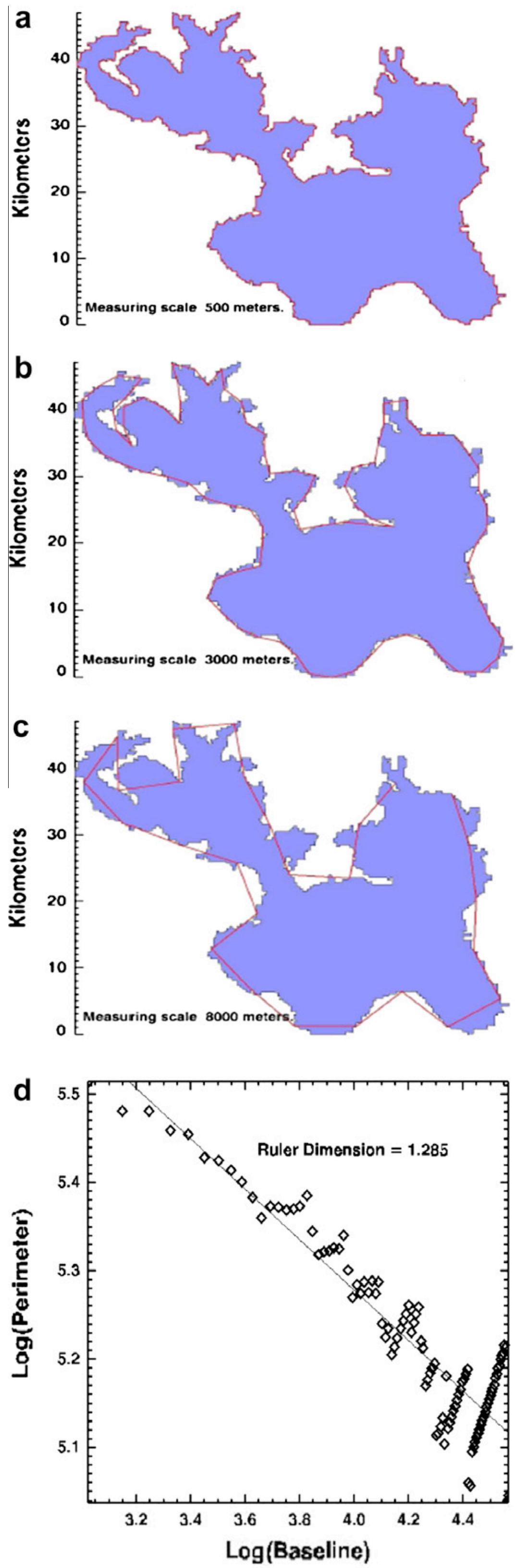

Fig. 7. The perimeter of one of Titan's lakes measured at multiple scales – 500 m, 3000 m and 8000 m (ruler method). (*D*) shows a plot of perimeter versus measuring scale in log–log space. The slope (=1 − *D*) of the linear fit though these data can be used to determine the fractal dimension of the shoreline – which in this case is 1.285.

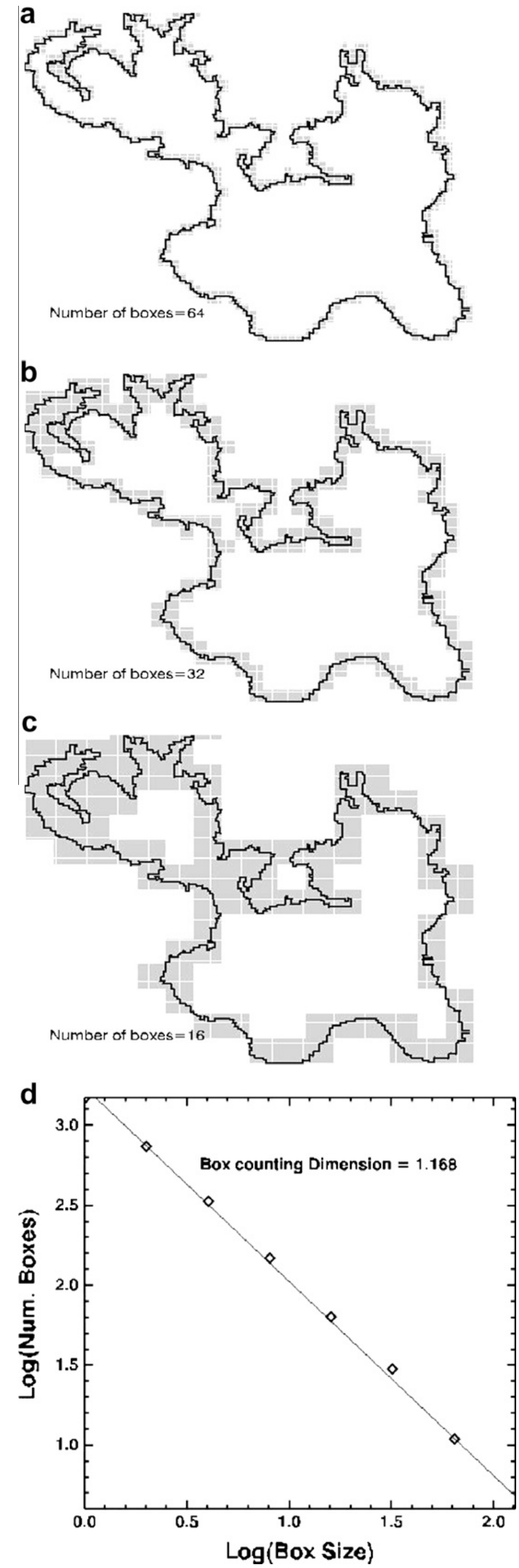

Fig. 8. The perimeter of one of Titan's lakes measured using different sizes of square boxes (box-counting method). (*D*) shows a plot of number of boxes versus measuring scale in log–log space. The slope (=−*D*) of the linear fit though these data can be used to determine the fractal dimension of the shoreline – which in this case is 1.168. The labels 'No. of boxes' refer to the number of rows and columns in the grid superimposed on the shoreline, e.g. 'No. of boxes' = 16 implies that a 16×16 grid was superimposed on the shoreline.

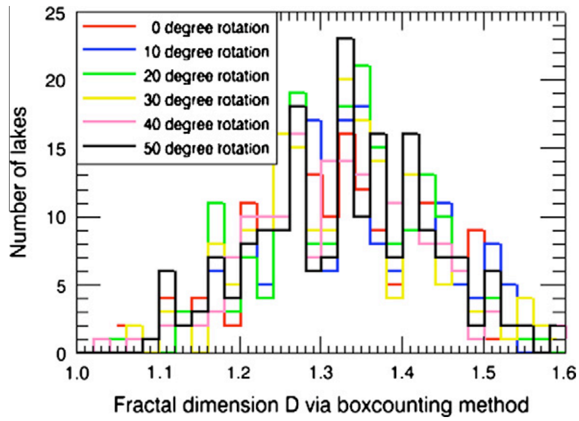

Fig. 9. Effect of rotation of lakes on calculation of box-counting fractal dimension.

thus, the fractal dimension of the landscape. Erosive processes like fluvial incision and aeolian erosion tend to increase the roughness of the landscape at smaller wavelengths, and thus the fractal dimension of the landscape/shoreline also increases. On the other hand, depositional processes like fluvial and aeolian deposition tend to smooth the landscape or decrease the roughness of the landscape at smaller wavelengths, thus decreasing the fractal dimension of the landscape. Similarly, the rate at which mass wasting (a diffusive process) occurs increases directly with slope of the landscape, which is highest over the shortest spatial scales. Thus, mass wasting smoothes small-scale roughness more efficiently than large-scale roughness and has an overall negative effect on the fractal dimension of the landscape. Mantling (fallout of solid tholin material from the atmosphere that blankets the surface) has a similar effect by smoothing the landscape and decreasing the fractal dimension. Tectonic activity can have a positive or negative effect on the fractal dimension of the landscape, depending on the scale of the surface features involved. Table 3 shows the effect of different kinds of surface processes on the fractal dimension of the landscape (Chase, 1992; Lifton and Chase, 1992).

Thus, in terms of interpreting the change in slopes of the plots for the multi-fractal shorelines, higher fractal dimensions would indicate dominance of erosive processes, while lower fractal dimensions can be associated with more widespread depositional processes. Detailed landscape evolution modeling in the future will help us to constrain which amongst a set of erosive/depositional processes could be responsible for a certain degree of increase/decrease in the fractal dimension.

4.2. Spatial variation of fractal dimension

Titan is a heterogeneous world, implying that surface processes which dominate in sculpting the landscape in one region need not do so in all regions. Such a spatial variation in surface processes could also show up as a distinct trend in the fractal dimension. We examined spatial variation of the fractal dimension of Titan's shorelines over latitude and longitude, employing both the ruler and the box-counting method.

In order to accomplish this, we calculated the fractal dimension of each lake via both the ruler and the box-counting method

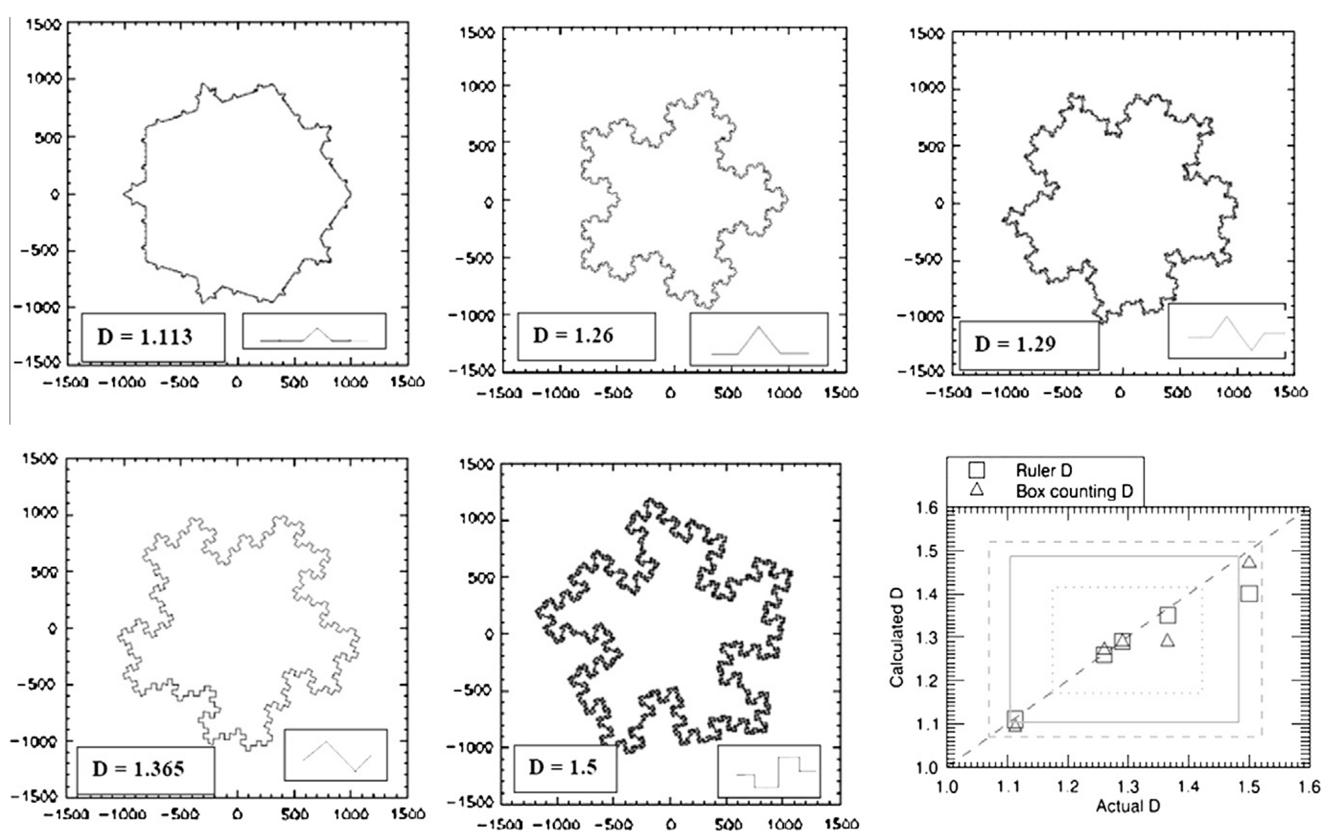

Fig. 10. Five synthetic fractals with known fractal dimensions were generated to test the accuracy of the ruler and box-counting methods. For each fractal, lower right inset shows the generator used for creating the fractal and lower left inset shows the theoretical dimension for the fractal. The scatter plot shows comparison of fractal dimensions of synthetic fractals calculated via ruler and box-counting method with the actual dimensions. The dotted gray line indicates 1σ range of dimensions for Titan's shorelines (1.17–1.42), the dashed gray line indicates the 2σ range (1.07–1.52) and the solid gray line indicates the 1.645σ range (1.1055–1.485).

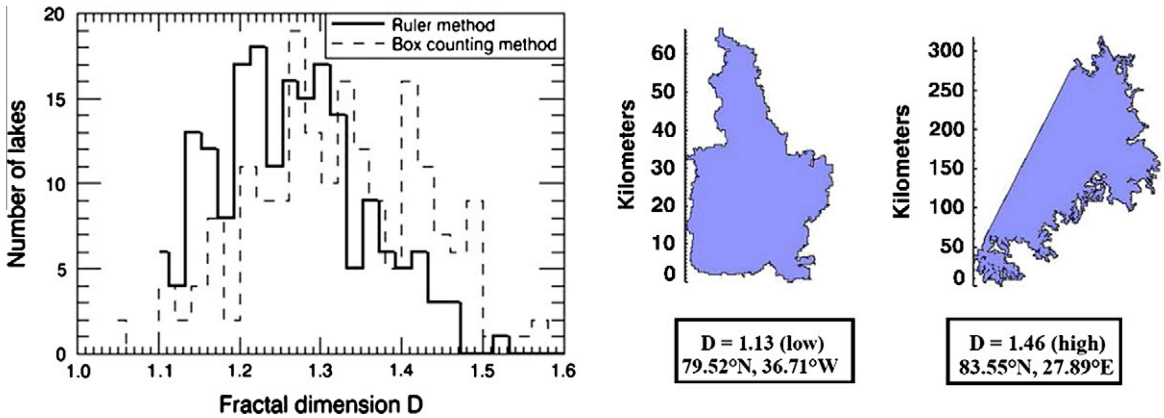

Fig. 11. Comparison of results of the ruler and box-counting analysis for Titan's north polar shorelines. The ruler method gives a mean fractal dimension of 1.27, while the box-counting method gives a value of 1.32. Examples of a smooth shoreline, with a low fractal dimension and of a rough and intricate shoreline, with a high fractal dimension are also shown.

and sorted them into 5° latitude and 30° longitude bins based on their median latitude/longitude. Fig. 13a–d shows the results of our spatial variation tests. In Fig. 13a–d, the labels show the number of lakes included in each band. In Fig. 13b and d, there is a sudden increase in the box-counting and ruler fractal dimension over the 60–90° longitude range, which is due to a single extremely intricate shoreline, and not due to a group of features. Although interesting, this single feature is not part of any larger trend.

To assess the significance of the fractal dimension variation with latitude and longitude we performed an analysis of variance (ANOVA) statistical test, which is a way of splitting the variance of the entire population into variance within sub-groups versus variance between groups. Results of this test are reported as an *F*-ratio, which can be converted into the probability that variability between groups occurs only by chance. A high value of the *F*-ratio indicates the different sub-groups are significantly different. A probability of occurrence by chance of 5% is considered the usual cutoff for statistical significance. Using the box-counting fractal dimensions in the 5° latitude bins, we derive an *F*-ratio of 1.07, which would occur by chance 37.4% of the time and with the 30° longitude bins, we derive an *F*-ratio of 1.14, which would occur by chance 33.3% of the time. Using the ruler fractal dimensions in the 5° latitude bins, we derive an *F*-ratio of 0.94, which would occur by chance 45.6% of the time and with the 30° longitude bins, we derive an *F*-ratio of 6.6, which would occur by chance <0.01% of the time. Thus there is no significant variation of fractal dimension with latitude with either method or longitude when using the box-counting method. The apparent variation of the ruler dimension with longitude is mostly due to a single lake at a longitude of 82°E (lake 36 in the Supplementary online material) with high fractal dimension (1.9). This lake is clearly an anomaly as its box-counting dimension is much lower (1.44). Excluding this lake reduces the *F*-ratio to 2.14, which one would still expect to occur by chance only 2.4% of the time. So the increased fractal dimensions of lakes in the (0–90)°E zone (where the largest lakes are located) shown in Fig. 13d could be considered statistically significant (although not overwhelmingly so). Possible explanations for this variability include variation in fluvial erosion due to regional variations in methane precipitation, variable aeolian erosion due to fluctuating wind activity or inconsistent mantling related to deviations in atmospheric structure/dynamics. Future work on detailed modeling of the surface processes that modify Titan's landscape would help us to more clearly identify the preponderance of certain processes over others in different regions.

4.3. Investigation for anisotropy

Certain surface processes like aeolian scour and tectonics can create directional topography. Variation of the fractal dimension of the landscape with direction can thus indicate the possibility that one or more of such processes might have modified the landscape. To test for anisotropy, we first rotated the lakes so that North was oriented upwards. Each lake was then split up into orthogonal N–S and E–W sections, such that there were equal number of vertices representing each direction (Fig. 14). We calculated fractal dimensions for the N–S ($D_{N/S}$) and E–W ($D_{E/W}$) sections via the box-counting and the ruler method and searched for systematic differences between the fractal dimensions of the orthogonal sections of each lake. These differences were then divided up into 2° latitude bands and 30° longitude bands.

Both the ruler and the box-counting method results imply a possible anisotropy in Titan's topography. Histograms of $D_{N/S} - D_{E/W}$ are skewed to negative values, with the ruler method results centered at −4.24% and spread out over a range of (−35 to 22)% and the box-counting results centered at −0.34% with a range of (−24 to 21)%. This indicates higher E–W section dimensions than N–S section dimensions (Fig. 15).

To assess the significance of the shift of the histograms shown in Fig. 15 away from the origin, we performed a two-tailed *t*-test. This test returns the probability that the null hypothesis is true, i.e. that the histograms in Fig. 15 are drawn from a population with a mean of zero (topography is isotropic) and that the non-zero mean we see has occurred only by chance. Results of this test are reported as a *t*-value, which (along with the number of degrees of freedom in the system) can be converted to this probability. For the distribution corresponding to the ruler method results, we calculated a *t*-value of −6.64, which would occur by chance <0.01% of the time if the null hypothesis were true. For the distribution corresponding to the box-counting method results, we calculated a *t*-value of −1.044, which would occur by chance 30% of the time if the null hypothesis were true. The box-counting results are not conclusive, as the anisotropy deduced from this distribution could easily have occurred by chance. However, the results from the *t*-test of the ruler distribution show that the chance that Titan's topography is isotropic is vanishingly small, thus the difference between the D_{NS} and D_{EW} is statistically significant. This result certainly warrants further investigation and will likely prove to be useful in better understanding the results of landscape evolution modeling in the future.

To test the effect of varying the orientation of the lakes on our results, we varied the orientation of the shorelines and performed

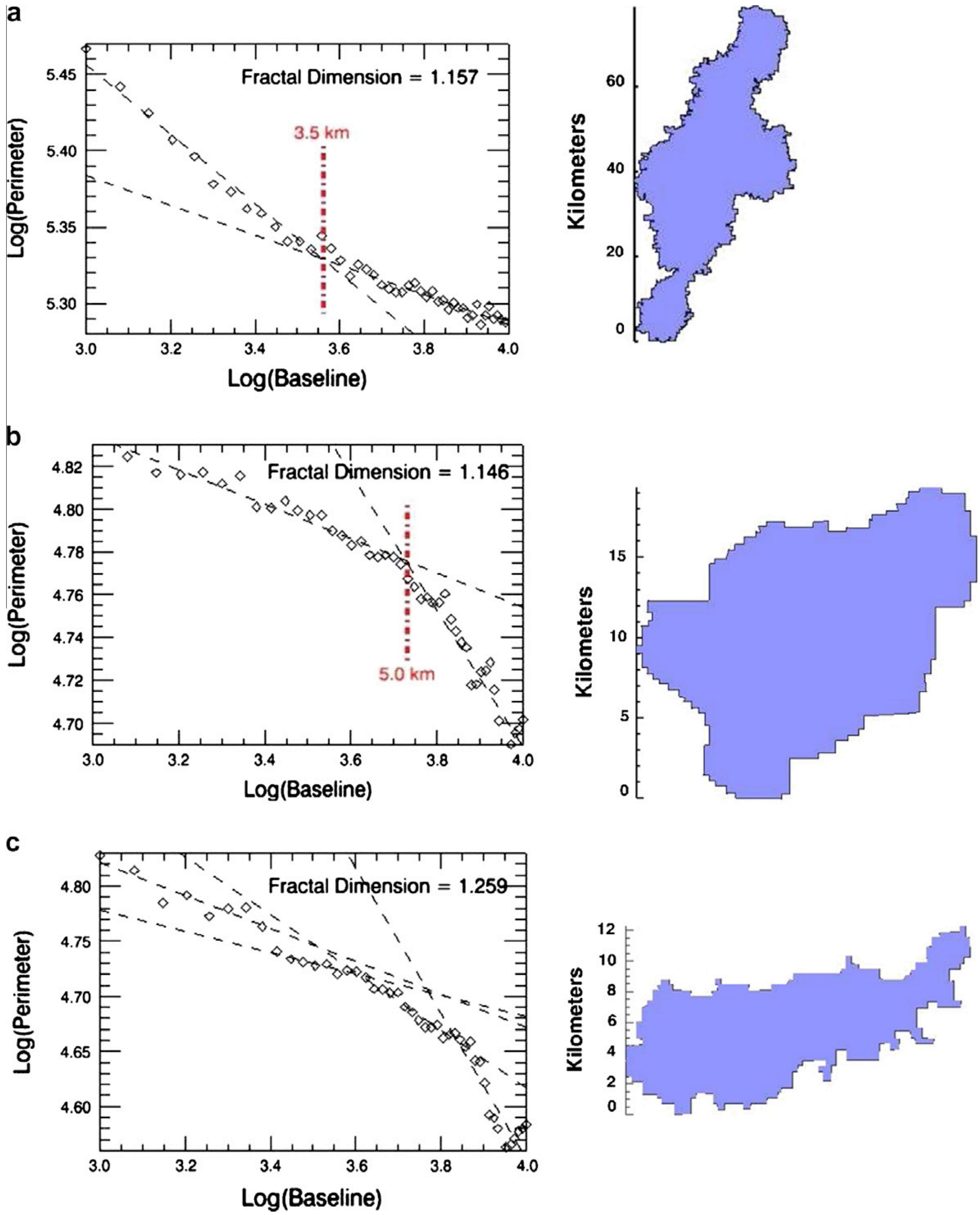

Fig. 12. Multifractal behavior exhibited by some of the lake shorelines, indicated by breaks in slopes of the powers spectra. Some shorelines, like the one in (C), exhibit multiple breaks in slope.

Table 3
Effect of different surface processes on fractal dimension of landscape.

Surface process	Effect on landscape/topography	Effect on fractal dimension
Fluvial erosion	Roughening	Increase (↑)
Fluvial deposition	Smoothing	Decrease (↓)
Mass wasting	Smoothing	Decrease (↓)
Tectonics	Roughening/smoothing (scale dependent)	Increase (↑)/decrease (↓) (scale dependent)
Aeolian deposition	Smoothing	Decrease (↓)
Mantling (atmospheric fallout)	Smoothing	Decrease (↓)

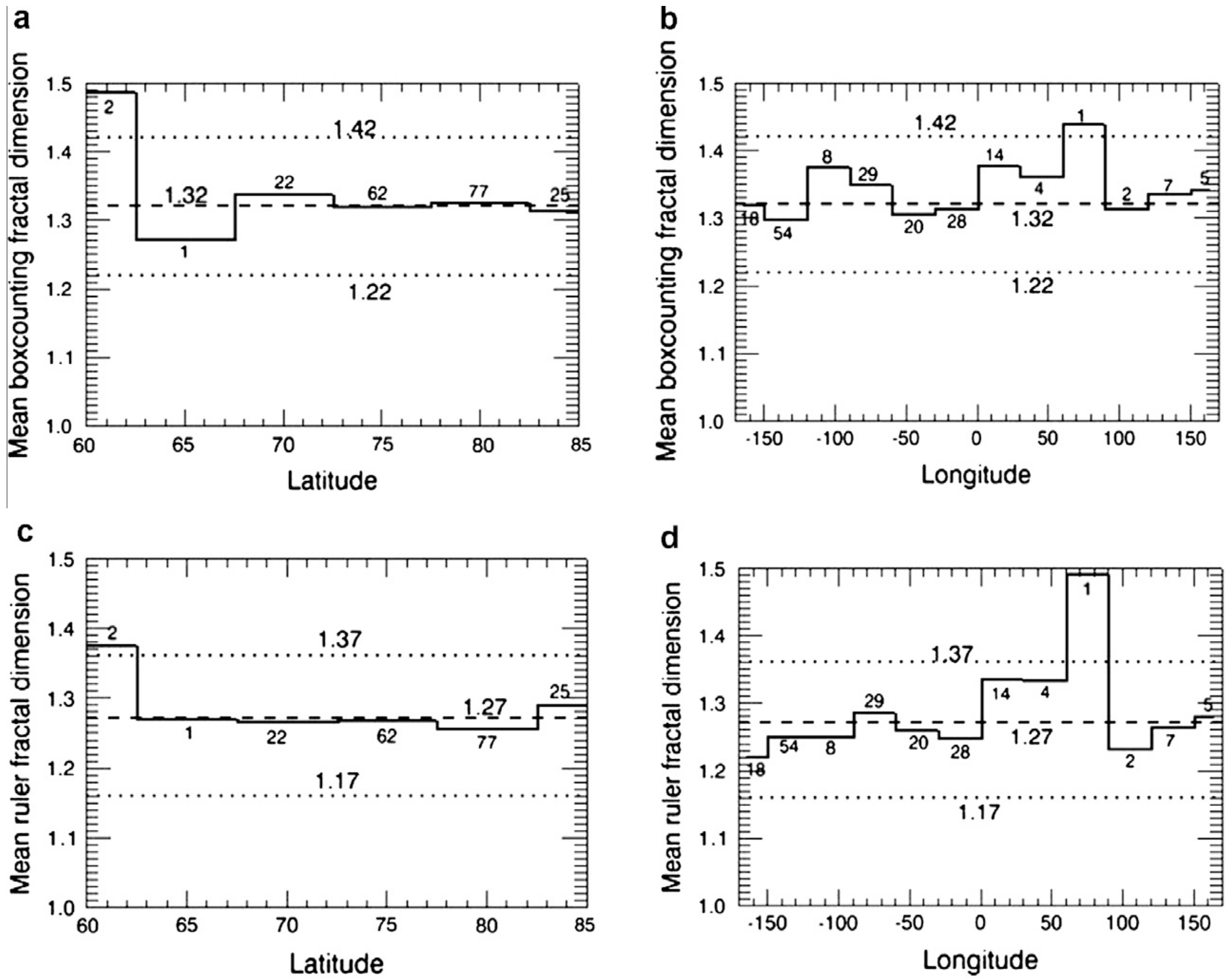

Fig. 13. (A and B) Variation of box-counting fractal dimension of the shorelines with latitude and longitude. (C and D) Variation of ruler fractal dimension of the shorelines with latitude and longitude. East longitudes are used. The labels show the number of lakes included in each band. The dashed lines denote the mean values of the fractal dimension over all bands, while the dotted lines denote the standard deviation from the mean.

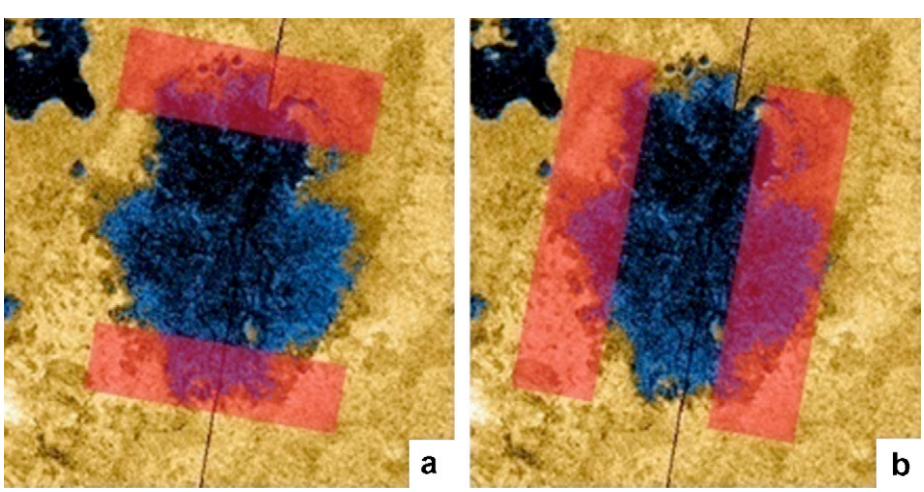

Fig. 14. One of Titan's north polar lakes, Bolsena Lacus (about 100 km in diameter). Sections of shoreline orientated roughly East–West (highlighted in a) and North–South (highlighted in b) can be independently analyzed and compared to investigate anisotropy in Titan's topography.

a similar analysis for sections of shorelines oriented N–E versus S–W, N–W versus S–E, etc. These alternate orientations also showed evidence for anisotropy; however, anisotropy was most pronounced in the case of the N–S versus E–W sections. These results suggest a role for anisotropic surface processes in sculpting Titan's landscape.

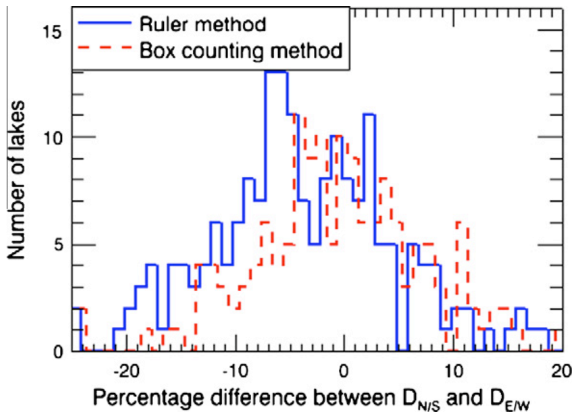

Fig. 15. Histograms of box-counting fractal dimensions and ruler fractal dimensions of North–South and East–West sections of shorelines at Titan's North Pole.

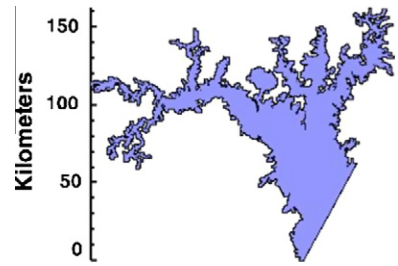

Fig. 17. Highly anisotropic shoreline of lake centered at 77.21°N, 82.07°E and with an area of ∼6900 km^2.

Fig. 16a–d shows variation in the percentage differences between dimensions of orthogonal sections over latitude and longitude. Vertical bars in the plots indicate 1σ of the range of values within each bin. The red dashed lines in the plots indicate 0% difference. We could not find any trends outside the general scatter of data in the plots. There is a sudden dip in the plots in Fig. 16b and d over the 60–90° longitude range, which is due to a highly anisotropic shoreline (corresponding to lake number 36 in the Supplementary online material). Interestingly, this complex shoreline centered at 77.21°N, 82.07°E and with an area of ∼6900 km^2 (Fig. 17) also shows up as the sudden increase in the fractal dimension over the 60–90° longitude range in our spatial variation plots (Fig. 13b and d).

5. Summary

We have carried out a fractal analysis of the shorelines of lakes at Titan's North Pole to extract information about Titan's topography. The statistical investigations undertaken until now provide us information only about relative relief. This paper does not describe

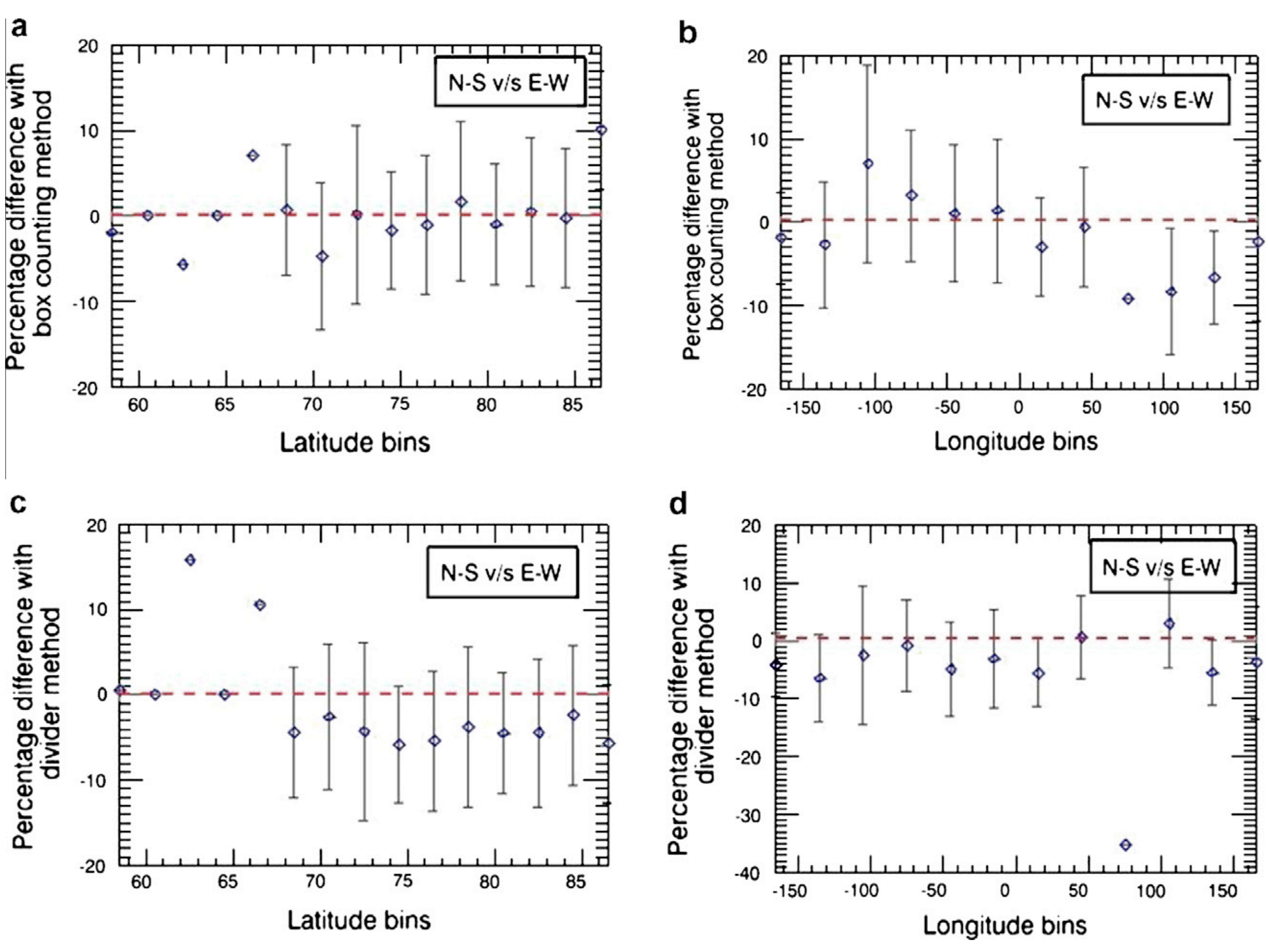

Fig. 16. Comparison of box-counting fractal dimensions and ruler fractal dimensions of orthogonal sections of shorelines over latitude and longitude. Vertical bars in the plots indicate 1σ of the range of values within each bin. East longitudes are used. Red dashed lines indicate 0% difference. (For interpretation of the references to color in this figure legend, the reader is referred to the web version of this article.)

the methods to quantify absolute relief, which will be the focus of future work.

The ruler method results were found to be more accurate and reliable than the box-counting results through comparisons to deterministic fractals. The ruler method results also bring to light the multi-fractal behavior of the titanian shorelines and the longitudinal variability of the fractal dimension as well as show a much stronger signature of anisotropic topography than the box-counting results, thus reinforcing our viewpoint that the ruler method is more precise.

The significant results of this study are listed here:

[1] The shorelines imaged at the North Pole of Titan by the Cassini RADAR can be described as self-similar fractals, similar to terrestrial coastlines. Their mean fractal dimensions (1.32 via box-counting and 1.27 via the ruler method) are similar to the dimensions of intricate terrestrial coastlines like the western coastline of Britain (1.25), which implies a rugged titanian landscape.

[2] Mean value of the slope (β) of the power spectra has been determined using both the theoretical relations as well as the empirical relations that we derived from the fractal analysis of the contours of synthetically generated power law surfaces. Using the mean of the ruler and box-counting dimensions (1.295), we obtain a value for theoretical β as 1.82 while the average empirical relation for a single contour gives a β value of 1.89. Using the more reliable of the two dimensions: the ruler dimension of 1.27, we get the theoretical/empirical value of β as 1.92/2.03. We thus conclude that Titan's β value could be lower than that of Earth and Venus (2.0). This may be due to Titan's lower gravity leading to lesser efficiency of diffusive (i.e. smoothing) processes, like mass wasting, on Titan.

[3] Some of the lake shorelines are found to exhibit multi-fractal behavior, with a few even displaying multiple breaks in slopes of the power spectra. This implies dominance of different surface processes at different spatial scales, with the transition scale between different fractal dimensions varying from (2–3.5) km for the larger lakes (area >250 km^2) and (2.2–7) km for the smaller lakes.

[4] We did not observe any spatial variation in the fractal dimension with latitude; however we do report significant spatial variation of the fractal dimension with longitude (increased fractal dimension in the 0–90°E zone where the largest lakes are located).

[5] There is a systematic difference between the ruler as well as box-counting method-derived dimensions of orthogonal sections of lake shorelines, which signifies possible anisotropy in Titan's topography. This asymmetry is the most pronounced in the case of the N–S versus E–W sections. These results seem to indicate modification of the landscape at the North Pole of Titan by anisotropic surface processes like aeolian scour or tectonism.

In the future, we intend to use the results of this fractal analysis to constrain the spatial distribution of surface process types on Titan and perform landscape evolution modeling to infer the dominant surface processes that sculpt the landscape of Titan.

Acknowledgments

The authors gratefully acknowledge those who designed, developed and operate the Cassini–Huygens mission. We also wish to thank Oded Aharonson, Sarah Hörst and an anonymous referee for useful comments.

Appendix A. Supplementary material

Supplementary data associated with this article can be found, in the online version, at doi:10.1016/j.icarus.2010.04.023.

References

Andrle, R., 1992. Estimating fractal dimension with the divider method in geomorphology. Geomorphology 5, 131–141.
Appleby, S., 1996. Multifractal characterization of the distribution pattern of the human population. Geogr. Anal. 28, 147–160.
Barnes, J.W., and 19 colleagues, 2007. Near-infrared spectral mapping of Titan's mountains and channels. J. Geophys. Res. (Planets) 112, E11006.
Brown, R.H., and 21 colleagues, 2004. The Cassini Visual and Infrared Mapping Spectrometer (VIMS) investigation. Space Sci. Rev. 115, 111–168.
Brown, R.H., Soderblom, L.A., Soderblom, J.M., Clark, R.N., Jaumann, R., Barnes, J.W., Sotin, C., Buratti, B., Baines, K.H., Nicholson, P.D., 2008. The identification of liquid ethane in Titan's Ontario Lacus. Nature 454, 607–610.
Chase, C., 1992. Fluvial landsculpting and the fractal dimension of topography. Geomorphology 5, 39–57.
Collins, G.C., 2005. Relative rates of fluvial bedrock incision on Titan and Earth. Geophys. Res. Lett. 32, L22202.
Elachi, C., and 21 colleagues, 2004. Radar: The Cassini Titan Radar Mapper. Space Sci. Rev. 115, 71–110.
Elachi, C., and 34 colleagues, 2006. Titan Radar Mapper observations from Cassini's T3 fly-by. Nature 441, 709–713.
Hayes, A., and 13 colleagues, 2008. Hydrocarbon lakes on Titan: Distribution and interaction with a porous regolith. Geophys. Res. Lett. 35, L09204.
Khare, B.N., and 10 colleagues, 1984. The organic aerosols of Titan. Adv. Space Res. 4, 59–68.
Klinkenberg, B., 1994. A review of methods used to determine the fractal dimension of linear features. Math. Geol. 26, 23–46.
Kondev, J., Henley, C.L., 1995. Geometrical exponents of contour loops on random Gaussian surfaces. Phys. Rev. Lett. 74, 4580–4583.
Kondev, J., Henley, C.L., Salinas, D.G., 2000. Nonlinear measures for characterizing rough surface morphologies. Phys. Rev. E (Statistical Physics, Plasmas, Fluids, and Related Interdisciplinary Topics) 61, 104–125.
Kucinskas, A.B., Turcotte, D.L., 1994. Isostatic compensation of equatorial highlands on Venus. Icarus 112, 104–116.
Lifton, N.A., Chase, C.G., 1992. Tectonic, climatic and lithologic influences on landscape fractal dimension and hypsometry: Implications for landscape evolution in the San Gabriel Mountains, California. Geomorphology 5, 77–114.
Longley, P.A., Batty, M., 1989. On the fractal measurement of geographical boundaries. Geogr. Anal. 21, 47–67.
Lopes, R.M.C., and 43 colleagues, 2007. Cryovolcanic features on Titan's surface as revealed by the Cassini Titan Radar Mapper. Icarus 186, 395–412.
Lorenz, R.D., Radebaugh, J., 2009. Global pattern of Titan's dunes: Radar survey from the Cassini prime mission. Geophys. Res. Lett. 36, L03202.
Lorenz, R.D., and 39 colleagues, 2006. The sand seas of Titan: Cassini RADAR observations of longitudinal dunes. Science 312, 724–727.
Lorenz, R.D., and 11 colleagues, 2007. Titan's young surface: Initial impact crater survey by Cassini RADAR and model comparison. Geophys. Res. Lett. 34, L07204.
Lunine, J.I., Atreya, S.K., 2008. The methane cycle on Titan. Nat. Geosci. 1, 159–164.
Malamud, B.D., Turcotte, D.L., 1999. Self-affine time series. I. Generation and analyses. Adv. Geophys. 40, 1–90.
Mandelbrot, B., 1967. How long is the coast of Britain? Statistical self-similarity and fractional dimension. Science 156, 636–638.
Mandelbrot, B., 1982. The Fractal Geometry of Nature. Freeman, San Francisco.
Mark, D.M., Aronson, P.B., 1984. Scale-dependent fractal dimensions of topographic surfaces: An empirical investigation with applications in geomorphology and computer mapping. Math. Geol. 16, 671–683.
Mitchell, K.L., Kargel, J.S., Wood, C.A., Radebaugh, J., Lopes, R.M.C., Lunine, J.I., Stofan, E.R., Kirk, R.L., and the Cassini Radar Team, 2007. Titan's crater lakes: Caldera vs. karst. Lunar Planet. Sci. 38, 2064 (abstracts).
Paillou, P., and 9 colleagues, 2008. Microwave dielectric constant of liquid hydrocarbons: Application to the depth estimation of Titan's lakes, Geophys. Res. Lett. 35, L05202.
Radebaugh, J., Lorenz, R.D., Kirk, R.L., Lunine, J.I., Stofan, E.R., Lopes, R.M.C., Wall, S.D., and the Cassini Radar Team, 2007. Mountains on Titan observed by Cassini Radar. Icarus 192, 77–91.
Radebaugh, J., and 15 colleagues, 2008. Dunes on Titan observed by Cassini Radar. Icarus 194, 690–703.
Rapp, R.H., 1989. The decay of the spectrum of the gravitational potential and the topography for the Earth. Geophys. J. Int. 99, 449–455.
Richardson, L.F., 1961. General Systems Yearbook, vol. 6, p. 139.
Sharma, P., Byrne, S., 2008a. Constraints on Titan's topography through fractal analysis of shorelines. In: AGU Fall Meeting, p. A1320 (abstracts).
Sharma, P., Byrne, S., 2008b. Constraints on Titan's topography through fractal analysis of shorelines. Lunar Planet. Sci. 39, 2145 (abstracts).
Soderblom, L.A., and 18 colleagues, 2007. Topography and geomorphology of the Huygens landing site on Titan. Planet. Space Sci. 55, 2015–2024.
Stiles, B., 2005. Cassini Radar Basic Image Data Records. SIS, JPL D-27889.
Stofan, E.R., and 37 colleagues, 2007. The lakes of Titan. Nature 445, 61–64.

Tatsumi, J., Yamauchi, A., Kono, Y., 1989. Fractal analysis of plant root systems. Ann. Bot. 64, 499–503.
Tomasko, M.G., and 39 colleagues, 2005. Rain, winds and haze during the Huygens probe's descent to Titan's surface. Nature 438, 765–778.
Turcotte, D.L., 1997. Fractals and Chaos in Geology and Geophysics, second ed. Cambridge University Press, Cambridge.
Turtle, E.P., Perry, J.E., McEwen, A.S., DelGenio, A.D., Barbara, J., West, R.A., Dawson, D.D., Porco, C.C., 2009. Cassini imaging of Titan's high-latitude lakes, clouds, and south-polar surface changes. Geophys. Res. Lett. 36, 2204.
Voss, R., 1988. Fractals in Nature: From characterization to simulation. In: Peitgen, Heinz-Otto, Saupe, Dietmar (Eds.), The Science of Fractal Images. Springer Press, pp. 21–70.